JPR Advance Access published July 8, 2016

Journal of
Plankton Research

plankt.oxfordjournals.org

J. Plankton Res. (2016) 00(00): 1–18. doi:10.1093/plankt/fbw047

Optimality-based *Trichodesmium* diazotrophy in the North Atlantic subtropical gyre

B. FERNÁNDEZ-CASTRO[1]*, M. PAHLOW[2], B. MOURIÑO-CARBALLIDO[1], E. MARAÑÓN[1] AND A. OSCHLIES[2]

[1]DEPARTAMENTO DE ECOLOXÍA E BIOLOXÍA ANIMAL, UNIVERSIDADE DE VIGO, 36310, VIGO, SPAIN AND [2]GEOMAR HELMHOLTZ CENTRE FOR OCEAN RESEARCH KIEL, KIEL, GERMANY

*CORRESPONDING AUTHOR: bieito.fernandez@uvigo.es

Received April 30, 2015; accepted June 4, 2016

Corresponding editor: Pia Moisander

A recent optimality-based model for phytoplankton growth and diazotrophy was applied at two stations located in the oligotrophic western and the ultra-oligotrophic eastern subtropical North Atlantic. Contrary to the common view that diazotrophy is favoured by nitrogen (N) depletion relative to the Redfield equivalent of phosphorus (P), we find that optimality-based diazotrophy could explain N fixation in both regions in spite of relatively high N:P supply ratios. This is possible because the availability of an additional source of N for diazotrophs makes them strong competitors for P under oligotrophic conditions. The best reproduction of observations, especially of net primary production, is only achieved with preferential remineralization of P relative to N and atmospheric deposition. In line with observations, a higher rate of nitrogen fixation is predicted for the eastern site, owing to a larger niche for diazotrophs resulting from stronger oligotrophy and lower N:P supply ratios due to weaker atmospheric N deposition. Because the competitive advantage of diazotrophs under nutrient starvation diminishes with increasing supply N:P ratio, the predicted increase of atmospheric N deposition due to anthropogenic activity could negatively affect N_2 fixation in the Atlantic Ocean.

KEYWORDS: optimality-based model; nitrogen fixation; atmospheric deposition; preferential remineralization; subtropical North Atlantic

INTRODUCTION

The ocean is responsible for an annual photosynthetic fixation of ≈50 Pg of carbon, which represents about half of the global primary production (Field *et al.*, 1998). Carbon fixation by marine phytoplankton in the photic layer and its transport to the deep ocean, known as the biological carbon pump, plays a key role in the ocean–atmosphere CO_2 exchange, and hence affects climate

available online at www.plankt.oxfordjournals.org

© The Author 2016. Published by Oxford University Press. All rights reserved. For permissions, please email: journals.permissions@oup.com

Downloaded from http://plankt.oxfordjournals.org/ by guest on July 12, 2016

on time scales from decades to millennia. Despite their oligotrophic nature, due to their large expanse, the subtropical gyres are responsible for about 50% of the marine export production (Emerson *et al.*, 1997). In these regions, phytoplankton growth is limited by the scarcity of nutrients, mainly nitrogen (N) (Moore *et al.*, 2013; Arteaga *et al.*, 2014). This limitation, however, can be relieved by the supply of this nutrient into the surface ocean by means of N_2 fixation and atmospheric deposition. Together with upward mixing of nitrate from below, this supply ultimately constrains the amount of fixed carbon that can potentially be exported to the deep ocean (Beckmann and Hense, 2009). N_2 fixation by diazotrophs is generally considered the most important source of fixed N into the ocean, and is believed to compensate globally for the fixed-N loss through denitrification and anammox (Deutsch *et al.*, 2007). Numerous studies indicate that this process contributes significantly to the new N input in the oligotrophic ocean (Capone *et al.*, 2005; Mouriño-Carballido *et al.*, 2011; Painter *et al.*, 2013; Fernández-Castro *et al.*, 2015).

Despite its crucial role in the marine N cycle, the magnitude of global N_2 fixation by marine diazotrophs (Carpenter and Capone, 2008) and the mechanisms controlling its regional distribution (Luo *et al.*, 2014) are rather poorly constrained. The view of diazotrophy being tightly coupled to N loss implies a competitive advantage of diazotrophic over ordinary phytoplankton in waters with excess phosphorus (P) relative to the Redfield equivalent of dissolved inorganic nitrogen (DIN) (Deutsch *et al.*, 2007). Accordingly, most of the marine N_2 fixation should take place in areas close to hot-spots of N loss. However, this is at odds with field observations indicating high abundances of the non-heterocystous diazotrophic cyanobacterium *Trichodesmium* sp. in the relatively nitrate-rich waters of the western central North Atlantic, which support high rates of N_2 fixation (Capone *et al.*, 2005; Luo *et al.*, 2012). Indeed, the nitrate excess observed in the thermocline of this region has been usually attributed to diazotrophic activity (Gruber and Sarmiento, 1997; Hansell *et al.*, 2004). Physiological requirements of *Trichodesmium* sp. such as warm, well-stratified and iron-replete waters to satisfy the high demands on energy and iron for nitrogenase, might partly explain the observed distribution (Carpenter, 1983; Moore *et al.*, 2009; Fernández *et al.*, 2010) and the spatial decoupling between fixed-nitrogen sinks and sources (Landolfi *et al.*, 2013). More recently other mechanisms, mainly preferential remineralization of phosphorus (Wu *et al.*, 2000; Monteiro and Follows, 2012) and atmospheric deposition of N of anthropogenic origin (Zamora *et al.*, 2010), have been identified as potential contributors to this phenomenon. However, a satisfactory explanation of the extent of diazotrophy in nitrogen-rich environments relative to phosphorus, such as the subtropical North Atlantic, is lacking.

Atmospheric fluxes of anthropogenic N into the oceans are increasing (Duce *et al.*, 2008). According to the current understanding of favourable conditions for diazotrophy in the ocean, it could be expected that this additional source of fixed N, resulting in an increase in the N:P inorganic supply ratio, could allow ordinary phytoplankton to out-compete diazotrophs (Krishnamurthy *et al.*, 2007; Zamora *et al.*, 2010). Consistent with the hypothesis of iron or phosphorus limitation of diazotrophy, N_2 fixation has been observed to respond positively to the addition of Saharan dust to natural water samples from the eastern subtropical Atlantic (Mills *et al.*, 2004; Moore *et al.*, 2013). However, negative responses of N_2 fixation to atmospheric N deposition have also been reported (Guieu *et al.*, 2014).

Optimality-based models offer a new interpretation of the controls of diazotrophy in plankton communities, because conditions favourable for diazotrophy are not prescribed but emerge, indirectly, from trade-offs among energy and cellular resource requirements for the acquisition of P, N and carbon. In this study we apply an optimality-based model of phytoplankton growth and diazotrophy (Pahlow *et al.*, 2013), as part of a complete optimality-based ecosystem model (Pahlow *et al.*, 2008), to two sites located in the ultra-oligotrophic eastern (25° N 30°W, NASE) and the oligotrophic western (31°N 64° W, NASW) North Atlantic subtropical gyre. Both areas are characterized by moderate N_2 fixation activity (Orcutt *et al.*, 2001; Painter *et al.*, 2013). The NASW site coincides with the location of the Bermuda Atlantic Time-series Study (BATS) site south of the Gulf Stream, in an area of relatively high N:P ratios in the upper thermocline (Fig. 1). The main goals of this study are: first to assess the performance of the optimality-based diazotrophy model under different levels of oligotrophy and N:P supply ratios in the subtropical North Atlantic and second to investigate the role of N_2 fixation and its interactions with atmospheric N deposition and preferential P remineralization at both sites.

METHOD

Adaptation of the plankton model

The plankton model used in this study is a modified version of the model described in Pahlow *et al.* (2008), which has been extended to cover dissolved and particulate phosphorus (P) dynamics (Fig. 2). Only the two main macronutrients (N and P) in inorganic and organic forms

Downloaded from http://plankt.oxfordjournals.org/ by guest on July 12, 2016

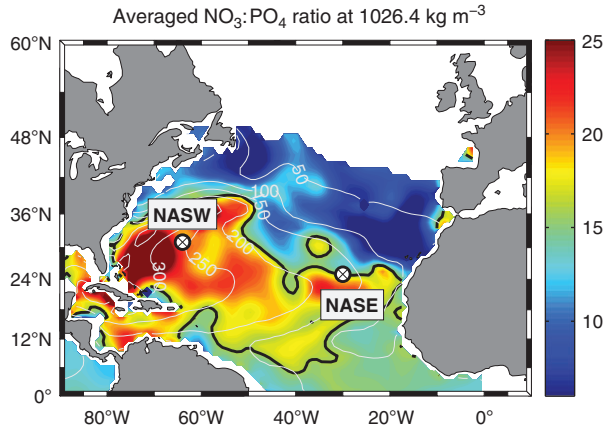

Fig. 1. Locations of the two sites in the western (NASW) and eastern (NASE) subtropical North Atlantic used for our model simulations and the EUMELI station. The location of NASW coincides with the location of the Bermuda Atlantic Time-series Study (BATS). The background color represents the averaged nitrate to phosphate (NO_3:PO_4) ratios on the 1026.4 kg m^{-3} isopycnal (located at 275 m and 81 m at the NASW and NASE sites, respectively). The black and white contour lines indicate the Redfield N:P (=16) ratio and the depth of the 1026.4kg m^{-3} isopycnal, respectively. Nutrient data were obtained from the World Ocean Atlas 2009 (Garcia *et al.*, 2010).

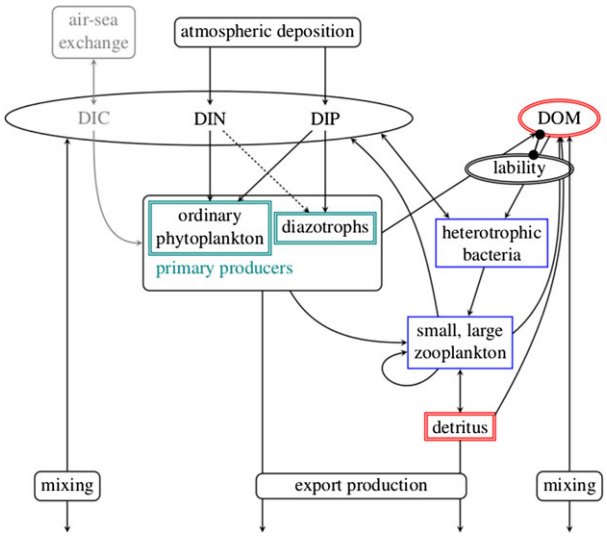

Fig. 2. Optimality-based ecosystem model of plankton and dissolved organic matter (DOM) dynamics. The model contains optimality-based formulations for primary production, N_2 fixation, zooplankton foraging, and heterotrophic bacterial dynamics. Phytoplankton, DOM, and detritus contain separate states for C, N, and P (double lines), whereas heterotrophic bacteria and zooplankton have fixed C:N:P composition. Diazotrophs can switch between N_2 fixation and DIN uptake (dashed arrow). Zooplankton fecal pellets are the sole source of detritus. Bacteria can potentially utilise or release inorganic N and P, depending on the C:N:P ratio of labile DOM. Labilities (labile fractions) of DOC, DON, DOP are represented by dynamic traits. Phytoplankton and detritus sink passively (export production). Air-sea exchange of CO_2 and water column carbonate chemistry are not explicitly simulated.

are considered. The distinction between organic and inorganic nutrients is defined operationally here, so that dissolved inorganic nutrients (DIN, DIP) are utilizable by both phytoplankton and heterotrophic bacteria, whereas organic nutrients (DON, DOP) are available exclusively to heterotrophic bacteria. Although iron availability might potentially limit diazotrophs, we assume that atmospheric deposition suffices to prevent significant limitation by this nutrient in our study (Sañudo-Wilhelmy and Kustka, 2001; Jickells *et al.*, 2005). A second phytoplankton compartment has been added to represent facultative diazotrophs.

Both phytoplankton compartments are described by the optimality-based chain model of Pahlow *et al.* (2013), which describes the optimal regulation of phytoplankton variable C:N:P stoichiometry and photo-acclimation (optimal Chl:C ratio). Briefly, the chain model rests on the concept of ecological stoichiometry (Sterner and Elser, 2002) and trade-offs arising from P, N, and energy requirements of nutrient assimilation, CO_2 fixation and other cellular functions. The main requirement for P is in membranes and nucleic acids (mainly nucleus and ribosomes). The high P requirement for ribosomes implies that P limits N assimilation. N is needed for structural protein and enzymes and hence defines a limit for all biochemical processes, such as light harvesting, CO_2 fixation or nutrient uptake. Thus, P and N form a chain of limitations, where P limits N assimilation and N limits growth. Diazotrophs have access to the practically unlimited supply of N_2. Although more expensive than DIN acquisition, diazotrophy is advantageous under oligotrophic conditions, as the high N supply facilitates not only CO_2 fixation. Because diazotrophs can devote more cellular N to P acquisition, diazotrophy also raises the competitive ability for DIP uptake compared to non-diazotrophs. See Pahlow *et al.* (2013) for details.

Model parameters for non-diazotrophic and diazotrophic phytoplankton were obtained from calibrations to chemostat experiments (Pahlow *et al.*, 2013). Diazotrophic phytoplankton parameters were calibrated to represent the observed behaviour of *Trichodesmium* sp., likely the main contributor to autotrophic N_2 fixation in the subtropical North Atlantic (Capone *et al.*, 2005). The model of Pahlow *et al.* (2013) was slightly modified to describe effects of temperature (T) on the phytoplankton maximum-rate parameter (V_0^P), the phytoplankton light-absorption coefficient (α^P) and the cost of chlorophyll maintenance (R_M^{chl}) by multiplying these parameters with a temperature factor as described in Pahlow *et al.* (2008). Since the parameter settings for *Trichodesmium* in Pahlow and Oschlies (2013) result in N_2 fixation occurring too deep in the water column, some phytoplankton parameters (Table S1) were adjusted to obtain a more realistic model behaviour.

Downloaded from http://plankt.oxfordjournals.org/ by guest on July 12, 2016

Zooplankton is described by an optimality-based model for zooplankton foraging (Pahlow and Prowe, 2010). Temperature effects are treated by multiplying the maximum ingestion rate and maintenance respiration parameters with a temperature function as suggested by Pahlow and Prowe (2010). As in Pahlow *et al.* (2008), zooplankton comprises two size classes described by the fraction of small zooplankton and total zooplankton biomass. Parameters for small and large zooplankton are based on the pre-calibrated parameter sets of Pahlow and Prowe (2010) for dinoflagellates and copepods, respectively (Table S1). Zooplankton maintains a constant C:N:P ratio and thus excretes or respires excess C, N, or P when ingesting food with a different effective C:N:P ratio.

Heterotrophic bacteria, detritus and dissolved organic matter (DOM) have been modified from Pahlow *et al.* (2008) and extended to account for P dynamics. Bacterial N and P dynamics are described by a chain-model approach, analogous to the phytoplankton compartments, except that instantaneous acclimation and constant C:N:P composition are assumed. Bacteria can supplement the dissolved organic P (DOP) associated with labile dissolved organic carbon (DOC) with additional uptake of DIP. Potential bacterial (combined inorganic and organic) P acquisition drives potential DIN uptake ($\hat{V}^{\mathrm{B}}_{\mathrm{DIN}}$):

$$\hat{V}^{\mathrm{B}}_{\mathrm{P}}=\left[\frac{1}{V^{\mathrm{B}}_{\max}\,Q_{\mathrm{P}}^{\mathrm{B}}}+\frac{1}{A^{\mathrm{B}}_{\mathrm{P}_i}P_{\mathrm{i}}}\right]^{-1}+V^{\mathrm{B}}_{\mathrm{P_{DOM}}},\ V^{\mathrm{B}}_{\mathrm{P_{DOM}}}=V^{\mathrm{B}}_{\mathrm{C}}Q_{\mathrm{P}}^{\mathrm{lDOM}} \tag{1}$$

$$\hat{V}^{\mathrm{B}}_{\mathrm{N}}=\hat{V}^{\mathrm{B}}_{\mathrm{P}}\frac{Q_{\mathrm{N}}^{\mathrm{B}}}{Q_{\mathrm{P}}^{\mathrm{B}}} \tag{2}$$

where $\hat{V}^{\mathrm{B}}_{\mathrm{P}}$ is the potential combined DIP and DOP acquisition, $Q^{\mathrm{B}}_{\mathrm{N}}$ and $Q^{\mathrm{B}}_{\mathrm{P}}$ are bacterial N:C and P:C ratios, respectively, $V^{\mathrm{B}}_{\mathrm{PDOM}}$ is the DOP taken in due to coupling with DOC, $V^{\mathrm{B}}_{\mathrm{C}}$ is the DOC uptake, $Q_{\mathrm{P}}^{\mathrm{lDOM}}$ is the labile DOP:DOC ratio, and $A^{\mathrm{B}}_{\mathrm{P}_i}$ is the bacterial uptake affinity for inorganic phosphorus, P_i. Actual DIC and DIN uptake or remineralization and respiration are then calculated according to Pahlow *et al.* (2008) and actual DIP uptake or release is given by:

$$V^{\mathrm{B}}_{\mathrm{P_i}}=(V^{\mathrm{B}}_{C}-R^{\mathrm{B}}_{C})Q_{\mathrm{P}}^{\mathrm{B}}-V^{\mathrm{B}}_{\mathrm{DOM}} \tag{3}$$

Model runs

The model was run off-line, forced with hourly vertical profiles of temperature and eddy-diffusion coefficients supplied from a 3D circulation model for the North Atlantic (Oschlies and Garçon, 1999) at 25°N 30°W (NASE) and 31°N 64°W (NASW) for the 12-year period from 01.01.1989 to 31.12.2001. The vertical profiles were obtained from all levels from the sea-floor (3000 m at NASW and 3500 m at NASE) to the sea-surface of the circulation model, with increasing resolution towards the surface. Predicted temperatures and mixed-layer depths in the 3D model deviate somewhat from the observations, most notably for NASE (Fig. 3a,e,i and m). However, predicted amplitude and seasonality of these parameters are essentially correct, as is the important feature that winter mixing extends below the nitracline at NASW but not at NASE (Fig. 3b,f,j and n). Thus, we consider the accuracy of the predictions of the 3D model sufficient to be used as boundary conditions for the present study. As shown below, it did indeed allow a qualitatively correct reproduction of the biogeochemistry at NASW and NASE (see also Fig. 3c,d,g,h,k,l,o and p).

We evaluate our model predictions following a 7-year spin-up with the same forcing as 1989. A spin-up of 7 years was chosen since longer spin-ups have only a minor influence on the model results compared to a 7-year spin-up. The bottom boundary (at 3000 m for NASW and 3500 m for NASE) was closed. Vertical velocities were not applied, as the problems caused by divergences arising from up- and downwelling could not be handled in a fully consistent manner in our one-dimensional (1D) model framework. Using a 1D model also means that we miss effects of horizontal transport. While we cannot quantify the uncertainties introduced by this omission, 1D models have been employed successfully in previous studies in the North Atlantic (e.g., Pahlow *et al.*, 2008; Salihoglu *et al.*, 2008; Mouriño-Carballido *et al.*, 2012). In fact, the 1D model of Salihoglu *et al.* (2008) showed the highest skill when compared to satellite-based and 3D models (Saba *et al.*, 2010). Similarly, Arteaga *et al.* (2015) also found that a restriction to local factors improved the estimation of surface nutrient concentrations. Thus, the better representation of local (biotic) processes in 1D models may outweigh the omission of lateral transport.

Model experiments for NASW were initialized with observed averaged (January) profiles from the BATS site for the period 1988–2012 (http://bats.bios.edu/). Unfortunately, no reference station exists in the ultra-oligotrophic NASE. For this reason model experiments at this site were initialized with averaged observed profiles from several cruises carried out in the NASE province (Marañón *et al.*, 2007; Fernández *et al.*, 2010, 2012; Mouriño-Carballido *et al.*, 2011). While not as close to the NASE location as these cruises, data from the oligotrophic site of the EUMELI project (21°N 31°W, http://www.obs-vlfr.fr/cd_rom_dmtt/eu_main.htm) have

Downloaded from http://plankt.oxfordjournals.org/ by guest on July 12, 2016

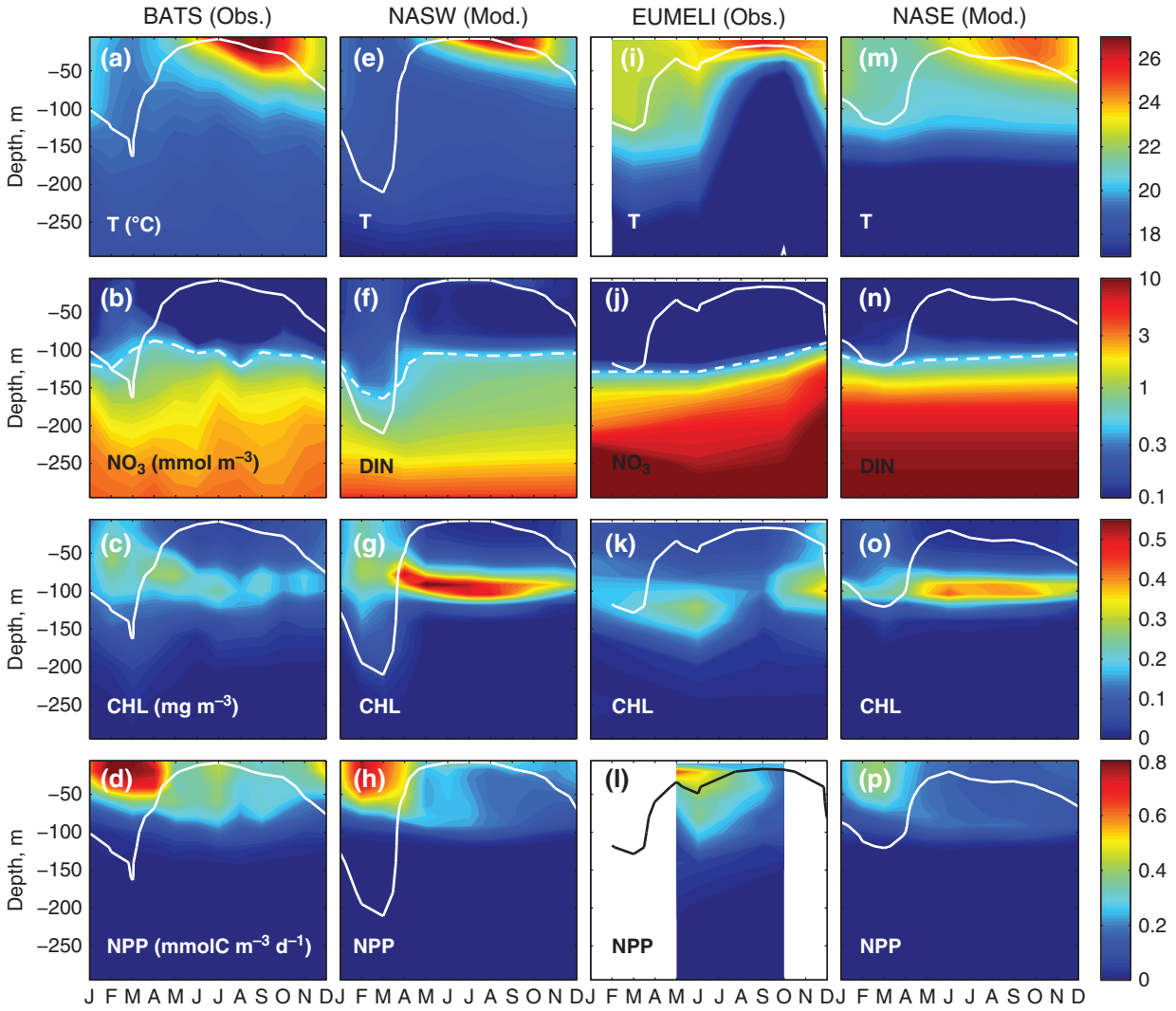

Fig. 3. Seasonal cycles (monthly climatologies) of Temperature (T, °C), dissolved inorganic nitrogen (DIN, mmolN m^{-3}), chlorophyll concentration (CHL, mg m^{-3}), and net primary production (NPP, mmolC m^{-3} d^{-1}) computed from model simulations (RDA configuration, including preferential remineralisation + diazotrophy + atmospheric N and P deposition) at the NASW (panels e–h) and NASE (panels m–p) model sites. Seasonal cycles derived from observations at the BATS site (panels a–d) and the oligotrophic site of the EUMELI project (panels i–l) are also included. Solid lines indicate climatological monthly mixed-layer depth computed using a temperature difference criteria of ΔT=0.5°C with respect to the surface. Dashed lines represent the nitracline depth (DIN = 0.5 mmol m^{-3}).

been used for model validation (see below). Unobserved quantities were calculated from assumed relations to observed quantities (Pahlow *et al.*, 2008).

In order to analyse the effects of diazotrophy, atmospheric deposition and preferential P remineralization and their interactions in these regions, sensitivity simulations were performed by running the model with and without these organisms/processes present. Model simulations with diazotrophic phytoplankton are labelled with a "D". In the other simulations these organisms are excluded by setting their initial concentration to zero. Simulations with atmospheric deposition of N and P, labelled with an "A", were carried out by supplying a constant flux of inorganic N and P into the surface model box of 11 m thickness. Estimates of present atmospheric N and P fluxes were obtained from Duce *et al.* (2008) and Mahowald *et al.*, (2008), respectively. N and P fluxes are 43 mol N m^{-2} d^{-1} and 0.091 mol P m^{-2} d^{-1} for BATS, and 12 mol N m^{-2} d^{-1} and 0.18 mol P m^{-2} d^{-1} for NASE. The N:P ratio of this atmospheric deposition is thus 473 and 67 for NASW and NASE, respectively, both substantially higher than the Redfield ratio. For this reason, although both N and P fluxes are included in the simulations, only the N flux is relevant for the results. While observations for temporally varying atmospheric deposition exist, they have little effect on our simulations,

Downloaded from http://plankt.oxfordjournals.org/ by guest on July 12, 2016

and they are lower on average for our simulation period (1989–2000) than the year-2000 estimates applied here for the present-day deposition fluxes. As this also greatly simplifies the analysis of the impact of future changes in atmospheric deposition (where the temporal distribution is unknown), we use a temporally constant deposition flux here for simplicity. Preferential P remineralization (labelled with an "R") is simulated by increasing by a factor of 2 the disintegration rate of detrital P to DOP (Letscher and Moore, 2015), and by reducing by the same factor the decline rate of DOP lability relative to that of DON (Fig. 2). Thus, in our model, P remineralization (to DIP) is affected only indirectly via providing more organic P to bacteria and hence, via bacterivory, to zooplankton, which then release the additional P as DIP.

As diazotrophy, atmospheric deposition and preferential P remineralization all affect the biogeochemical state of the North Atlantic subtropical gyre, we consider the RDA configuration, including all of these processes, as the reference simulation for comparison with observations.

RESULTS

Seasonal variability

The comparison of the observed and simulated seasonal cycles of temperature, dissolved inorganic N, chlorophyll and net primary production (NPP) for the reference RDA configuration shows that NASW is characterized by a winter mixing period with mixed-layer depths typically exceeding the nitracline depth (ca. 150 m) (Fig. 3a,b,e and f). As a result, nutrient entrainment causes an increase in primary production (Fig. 3c,d,g and h). During summer, the water column re-stratifies, primary production declines and a deep chlorophyll maximum (DCM) develops. The model is able to reproduce the general observed patterns for the NO_3, chlorophyll and NPP distributions. However, the peak values of chlorophyll at the DCM and of NPP during the late winter bloom are over and underestimated, respectively, by the model.

The seasonality of the NASE model output is characterized by a weaker seasonal forcing in comparison to the western location. Mixed layer depths are shallower in winter (≈120 m) and deeper in summer (≈50 m) (Fig. 3m). Due to the presence of nutrient-poor North Atlantic subtropical mode water at NASW (Steinberg *et al.*, 2001), the nitracline is steeper at NASE (Fig. 3n). However, weaker winter mixing at this station prevents significant penetration of the mixed layer below the nitracline depth. Although the main seasonal features observed at NASW, such as the winter–spring maximum in primary production and the formation of a DCM during summer stratification, are also observed at NASE, maximal values are lower reflecting the stronger oligotrophy at the eastern site. Monthly climatologies calculated from observations for the oligotrophic site of the EUMELI project show the seasonal cycles of temperature, NO_3, chlorophyll and NPP in comparison with our model predictions (Fig. 3i–p). Although the coarse resolution of these measurements makes the comparison somewhat difficult, the general patterns of the nutrient, chlorophyll and NPP distributions at NASE appear consistent with our model results, except the timing of the peak in NPP. Modelled depth-integrated chlorophyll concentration and NPP at the NASW site are compared with seasonal cycles of these quantities calculated from BATS data for the period 1989–2001 in Fig. 4a and b. Modelled depth-integrated chlorophyll and NPP show a maximum of about 30 mg m^{-2} and 50 mmol C m^{-2} d^{-1}, respectively, between February and April, in good agreement with the observations at the BATS site. Modelled integrated chlorophyll then declines from roughly 22 mg m^{-2} in May to 14 mg m^{-2} in December, within the range of the observations for this period. Hence, despite the overestimation of the peak chlorophyll concentration in the DCM, the model prediction roughly matches the observed depth-integrated chlorophyll values. Concurrently, modelled NPP declines from 26 to 28 mmol C m^{-2} d^{-1} to 18 mmol C m^{-2} d^{-1}, slightly below the corresponding averaged observed values of 27–40 mmol C m^{-2} d^{-1} (Fig. 4b), although the difference is not statistically significant.

The modelled chlorophyll at the NASE site shows much less seasonality, with a maximum of 19 mg m^{-2} in March and a minimum of 13.4 mg m^{-2} in December (Fig. 4c). The predicted pattern is compatible with data from several cruises carried out in the NASE region between 1992 and 2001 (Marañón *et al.*, 2007) and also with observations from the EUMELI project, both of which indicate much weaker seasonality at NASE compared to NASW. Modelled NPP is also maximal in March (31.5 mmol C m^{-2} d^{-1}) and declines to a minimum in December (15 mmol C m^{-2} d^{-1}), and is in good agreement with observations carried out between April and November in the NASE region (Fig. 4d). The few measurements available for the period from December to March indicate a stimulation of NPP, in line with the model results. In general, differences in the seasonal variability and values of chlorophyll and primary production at the two sites are in good agreement with previous studies on both sides of the North Atlantic (Steinberg *et al.*, 2001; Neuer *et al.*, 2007; Fernández-Castro *et al.*, 2012).

Downloaded from http://plankt.oxfordjournals.org/ by guest on July 12, 2016

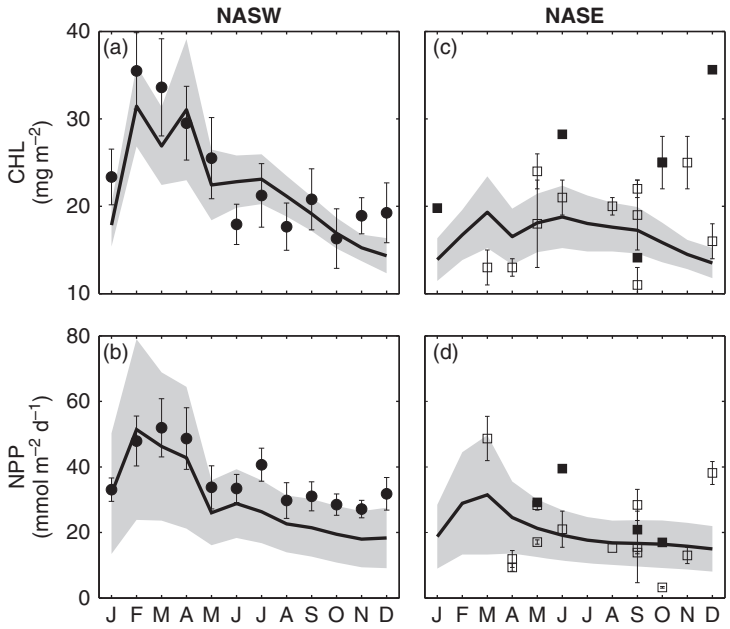

Fig. 4. Depth integrated monthly climatologies of chlorophyll concentration (CHL, mg m^{-2}) and net primary production (NPP, mmolC m^{-2} d^{-1}) computed from model simulations using the RDA configuration, including preferential remineralisation + diazotrophy + atmospheric N and P deposition (black thick line). Shadowed areas indicate standard deviations. Filled circles (●) represent seasonal cycles of NPP and CHL computed from BATS data (NASW), open squares (□) represent cruise measurements compiled in Marañón et al. (2007) at the NASE region and filled squares (■) represent averaged measurements from the oligotrophic site of the EUMELI project.

Modelled annual-mean depth-integrated chlorophyll for NASW and NASE (23.8 ± 5.1 and 17.1 ± 3.1 mg m^{-2}, respectively) agree well with observations from the BATS program for 1989–2001 (23.2 ± 3.7 mg m^{-2}) and NASE for March 1992 to November 2001 (Marañón *et al.*, 2007), respectively (see Table I). Since we do not consider vertical velocities in our simulations, we miss the associated NO_3^- and PO_4^{3-} fluxes into and out of the photic layer. Siegel *et al.* (1999) estimated the NO_3^- flux from episodic mesoscale eddy pumping as roughly 658 μmol m^{-2} d^{-1}, which is much higher than the total upward N flux in our model (~240 μmol m^{-2} d^{-1}). Sub-seasonal variations in surface DIN are indeed somewhat weaker in our model than in the BATS data (not shown), and our modelled annual NPP at NASW (29 ± 6.8 mmol C m^{-2} d^{-1}) is, albeit only slightly, lower than observations at BATS (36.5 ± 5.9 mmol C m^{-2} d^{-1}). A possible reason for such a weak effect of missing episodic vertical velocities may be that at NASW cyclonic eddies uplift water with relatively low Si^* (the relative abundance of silicate over nitrate), a signature that originated in the iron-limited Southern Ocean (Bibby and Moore, 2011). This phenomenon can explain the dominance of the phytoplankton community by small prokaryotic phytoplankton in cyclonic features in this region and, on average, no significant increases in primary production (Mouriño-Carballido, 2009). Modelled primary production of diazotrophs at this site is 0.32 ± 0.26 mmol C m^{-2} d^{-1}, about 1% of the total. Total simulated NPP at NASE (20.1 ± 6.9 mmol C m^{-2} d^{-1}) agrees with observations (20.3 ± 3.5 mmol m^{-2} d^{-1}, Marañón *et al.*, 2007). In this case, modelled NPP by diazotrophs is 0.67 ± 0.17 mmol C m^{-2} d^{-1}, about 2% of the total.

The model estimates of net community production (NCP) for NASW (6.5 mmol C m^{-2} d^{-1}) fall well within the range of estimates for BATS (Musgrave *et al.*, 1988; Marchal *et al.*, 1996; Gruber *et al.*, 1998; Brix *et al.*, 2006; Fernández-Castro *et al.*, 2012). Predicted NCP at NASE is less than half of that at BATS (2.5 mmol C m^{-2} d^{-1}). Biogeochemical estimates of NCP rates reported for the ESTOC site located in the eastern (more productive) end of the NASE province are somewhat lower than those reported for BATS (González-Dávila *et al.*, 2007; Fernández-Castro *et al.*, 2012; Cianca *et al.*, 2013). Furthermore, carbon export fluxes measured by sediment traps at ESTOC are 3–4 times lower compared to BATS (Helmke *et al.*, 2010).

The modelled seasonal cycle of depth-integrated N_2 fixation at NASW for the reference model configuration (RDA) shows minimal N_2 fixation in spring, increasing during summer towards a maximum in October, immediately below the mixed layer depth, and declining, although not to zero, during the winter mixing period

Downloaded from http://plankt.oxfordjournals.org/ by guest on July 12, 2016

Table I: Modelled and observed averaged variables for the western (NASW) and eastern (NASE) subtropical North Atlantic

	NASW (BATS)		NASE	
	Model	Observations	Model	Observations
Chl *a* (mg m^{-2})	23.8 ± 5.1	23.2 ± 3.7	17.1 ± 3.1	17 ± 1[a]
Total NPP (mmol m^{-2} d^{-1})	29.2 ± 6.8	36.5 ± 5.9	20.1 ± 6.9	20.33 ± 3.5[a]
NPP Diaz. (mmol m^{-2} d^{-1})	0.32 ± 0.26		0.67 ± 0.17	
NCP (mmol m^{-2} d^{-1})	6.5 ± 2.6	4.7–13.42[b]	2.5 ± 1.4	3.9–9.04[b]
Phyto. POC (mmol m^{-2})	241 ± 31		193 ± 28	116 ± 72[a]
Diaz. POC (mmol m^{-2})	1.7 ± 1.4		3.7 ± 0.59	
POC (mmol m^{-2})	391±59	234±79	310± 51	
PON (mmol m^{-2})	42.2 ± 7.1	33±12	33.7 ± 5.4	
POP (mmol m^{-2})	2.01 ± 0.34	1.19 ± 0.42	1.58 ± 0.28	
DOC (mmol m^{-2})	7750 ± 71	6015 ± 263	11 727 ± 1209	
DON (mmol m^{-2})	543 ± 3	420 ± 28	789 ± 81	
DOP (mmol m^{-2})	12.45 ± 0.04	8.1 ± 3.6	20.3 ± 2.0	
N_2 fixation (μmol m^{-2} d^{-1})	29 ± 23	29 ± 16[c]	49 ± 17	55.6 ± 8.0[c]
DIN flux (μmol m^{-2} d^{-1})	242 ± 95		109 ± 70	
Atmos. N deposition (μmol m^{-2} d^{-1})	43	43	12	12
Total N supply (μmol m^{-2} d^{-1})	314		170	
DIP flux (μmol m^{-2} d^{-1})	11.8 ± 4.5		5.4 ± 3.4	
Phyto. DIN uptake (μmol m^{-2} d^{-1})	1635 ± 472		1000 ± 390	
Phyto. DIP uptake (μmol m^{-2} d^{-1})	60 ± 18		37 ± 15	
Diaz. DIN uptake (μmol m^{-2} d^{-1})	0.17 ± 0.17		0.52 ± 0.46	
Diaz. DIP uptake (μmol m^{-2} d^{-1})	0.59 ± 0.47		1.00 ± 0.36	
N:P supply (Mix.)	20.6		20.1	
N:P supply (Mix.+Dep.)	24.3		21.7	
N:P supply (Mix.+Dep.+N2 fix.)	26.7		30.5	
Photic layer DIN:DIP	11.8	13[d]/24[e]	14.3	4.1[e]
Phyto. Uptake N:P	27.5		27.0	
Diaz. Fixation+Uptake N:P	49.4		49.5	
Phyto Biomass C:N	15.9		16.0	
Phyto. Biomass N:P	27.5		28.2	
Diaz. Biomass C:N	6.0	6.3–7.3[f]	6.3	6.3–7.3[f]
Diaz. Biomass N:P	50.3	60[g] / 34.2–44.8[f]	50.3	30[g] / 34.2–44.8[f]
POM C:N	9.26	7.2	9.26	
POM N:P	21.0	27.5	21	
DOM C:N	14.3	14.3	14.3	
DOM N:P	43.7	51.6	43.7	

Model simulations correspond to the reference RDA (including preferential remineralization + diazotrophy + prescribed atmospheric N and P deposition) configuration. Stocks and rates values correspond to depth integrations in the photic layer (determined as the deepest model bin where NPP > 0). NPP is net primary production; POC (PON/POP) is particulate organic carbon (nitrogen/phosphorus) concentration; DOC (DON/DOP) is dissolved organic carbon (nitrogen/phosphorus) concentration; Mix. is vertical mixing across the thermocline; and Dep., atmospheric deposition. Data for NASW are from the BATS site unless indicated.

[a]Marañón *et al.* (2007).

[b]Carbon budget estimates from Musgrave *et al.* (1988), Marchal *et al.* (1996), Gruber *et al.* (1998), Brix *et al.* (2006), González-Dávila *et al.* (2007), Fernández-Castro *et al.* (2012).

[c]Luo *et al.* (2012).

[d]$(NO_3 + NO_2)$:SRP, SRP: soluble reactive phosphorus.

[e]$(NO_3 + NO_2)$:PO_4.

[f]Letelier and Karl (1998) for *Trichodesmium* sp. colonies sampled at the HOT (Hawaii Ocean Time-series) station in the North subtropical Pacific.

[g]Krauk *et al.* (2006).

(Fig. 5g). This pattern is in close agreement with the marked seasonality reported for the *Trichodesmium* sp. colony abundance and N_2 fixation at the BATS site for the period 1995–1997 (Orcutt *et al.*, 2001), although somewhat different in magnitude (Fig. 5a). This difference might partly be due to fixation by free trichomes. For example, Orcutt *et al.* (2001) inferred from a few measurements of free trichome abundances that trichomes contribute a major fraction to the total N_2 fixation, with a maximum in August, slightly earlier than predicted by the model. In the model, the N_2 fixation maximum occurs at about 50 m, immediately below the mixed layer depth and above the DCM, whereas field observations indicate a strong decrease below the surface maximum.

Modelled annual-mean depth-integrated N_2 fixation for NASW, for the reference model configuration (29 ± 23 μmol N m^{-2} d^{-1}) is comparable with total (free trichomes + colonies) N_2 fixation reported by Orcutt

Downloaded from http://plankt.oxfordjournals.org/ by guest on July 12, 2016

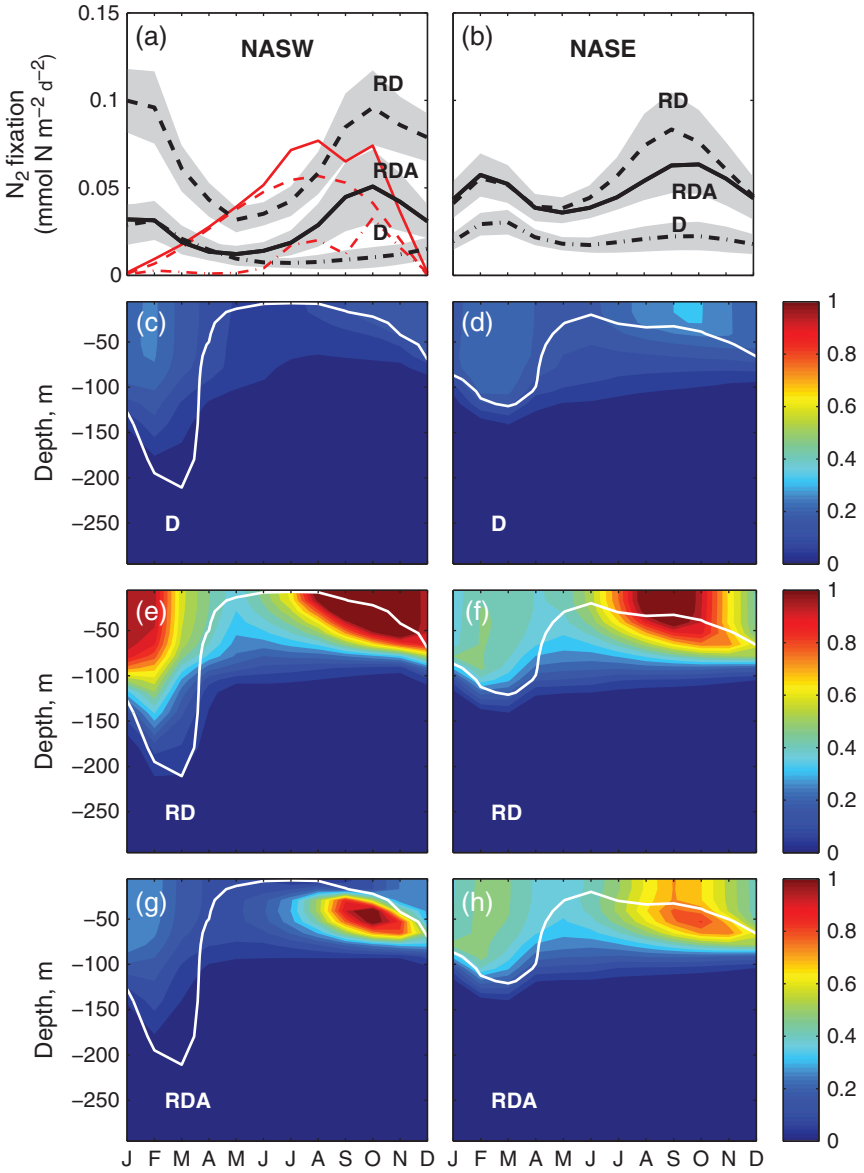

Fig. 5. Simulated seasonal cycles (monthly climatologies) of N_2 fixation for the RDA (preferential remineralisation + diazotrophy + atmospheric N and P deposition), RD (preferential remineralisation + diazotrophy) and D (diazotrophy) configurations. Panels a and b represent depth-integrated N_2 fixation values for the different model runs (black thick lines) at NASW and NASE, respectively. Shadowed areas represent the standard deviation. RedGray lines represent observations at the BATS site (Orcutt et al., 2001): N_2 fixation by *Trichodesmium* colonies (dash-dotted line), N_2 fixation by free trichomes (dashed line) and the sum of both (solid line). Depth-resolved seasonal cycles are shown in panels c-h. White lines indicate the mixed-layer depth computed using a temperature difference criteria of ΔT=0.5°C with respect to the surface.

et al. (2001) (40 μmol N m^{-2} d^{-1}), and in very good agreement with the averaged depth-integrated N_2 fixation rate calculated within a radius of 10° around BATS from the Luo *et al.*, (2012) compilation (29 ± 16 μmol N m^{-2} d^{-1}).

The reference simulation at the NASE site predicts the N_2 fixation maximum between September and October, also below the mixed layer, at about 50 m (Fig. 5b and h). However, the model also predicts weak N_2 fixation in the mixed layer during the winter mixing period. The minimum in this case is between April and June. Unfortunately, the limited existing observations are insufficient to establish the seasonality of N_2 fixation in this region. Modelled annual-mean depth-integrated N_2 fixation rate for NASE (49 ± 17 μmol N m^{-2} d^{-1}) is higher than for NASW, and in good agreement with the depth-integrated estimate obtained from the Luo *et al.* (2012) database (55.6 ± 8.0 μmol N m^{-2} d^{-1}, also

Downloaded from http://plankt.oxfordjournals.org/ by guest on July 12, 2016

calculated within a radius of 10° around the reference station for NASE).

Sensitivity of N_2 fixation to preferential P remineralization and atmospheric fluxes

The comparison of our model simulations shows that the predicted seasonal and vertical distribution of diazotrophy is sensitive to preferential remineralization of phosphorus and atmospheric deposition of N and phosphorus, for both NASW and NASE (Fig. 5). For the D (diazotrophy) configuration, depth-integrated N_2 fixation at NASW is minimal in July and increases towards a maximum in February during the winter mixing period (Fig. 5a and c). This seasonal structure is not consistent with the observed pattern. The RD (diazotrophy + preferential remineralization) model configuration produces generally higher depth-integrated N_2 fixation rates and the seasonal variability agrees better with the observations, as N_2 fixation peaks in October and starts declining when the mixed layer starts deepening (Fig. 5a). Significant N_2 fixation still occurs in January and February but volumetric rates are low compared to the summer–autumn maximum (Fig. 5e). When atmospheric N deposition is also included, the model is better capable of reproducing the observed seasonal patterns as depth-integrated N_2 fixation in winter is more strongly reduced in comparison with the summer (Fig. 5a). The seasonal variability of the modelled diazotrophic activity at NASE shows similar patterns as described for NASW, but autumn-time N_2 fixation is less important in relative terms compared to BATS.

The D and RD simulations show maximum N_2 fixation at the surface, decreasing rapidly with depth at both locations (Fig. 5), in agreement with the observations for the BATS site (Orcutt *et al.*, 2001). In the RDA simulation, the introduction of atmospheric N at the upper boundary displaces the N_2 fixation maximum deeper in the water column. This occurs because the enhanced N availability due to atmospheric deposition reduces the available niche for N_2 fixation at the surface.

Cellular resource allocation

Diazotrophs can access the inexhaustible pool of N_2 but this ability comes at the cost of having to allocate cellular resources in the form of energy and N (for the necessary enzymes) to the task of N_2 fixation. The optimality-based chain model of Pahlow *et al.* (2013) describes the allocation of cellular N among the requirements for CO_2 fixation, N_2 fixation, DIN uptake and DIP uptake, so that net growth is maximized. Owing to the high availability of N_2 gas, diazotrophs can afford to allocate a much smaller fraction of their cellular N to N acquisition (combined N_2 fixation and DIN uptake) than non-diazotrophs. Fig. 6 shows relative allocation in units of mol N mol $N,^{-1}$ but the patterns are very similar for absolute allocation in units of mol N mol C^{-1} (not shown), owing to the generally higher N demand of the diazotrophs. The sum of the allocations shown in Fig. 6 is less than one because it is only the allocation towards nutrient acquisition, with the remainder being allocated to light harvesting, CO_2 fixation and structural protein (not shown). At deeper layers, most of the cellular N is allocated towards light harvesting, resulting in only minor allocations for nutrient acquisition in Fig. 6. While non-diazotrophs allocate most of the N devoted to nutrient acquisition towards DIN uptake, diazotrophs need to allocate only a much smaller fraction of their cellular N towards N acquisition and hence can allocate more towards DIP uptake (Fig. 6). Their high N supply compared to non-diazotrophs in the oligotrophic waters of the NASW and NASE locations thus confers another strong advantage to the diazotrophs: a much improved ability to acquire and compete for DIP.

Atmospheric deposition and preferential remineralization of phosphorus

Fig. 7 illustrates the roles of atmospheric deposition and preferential phosphorus remineralization on NPP and diazotrophy at NASW and NASE. Including diazotrophy (D) at NASW causes an increase in NPP by about 44% with respect to the control configuration (0). NPP increases even more (by about 100%) when preferential phosphorus remineralization is also included together with diazotrophy (RD), but preferential remineralization alone (R) has no effect. Nevertheless, the diazotrophs themselves contribute less than 5% to the total NPP (Fig. 7, circled light coloured bars), indicating that N_2 fixation predominantly enhances NPP indirectly, by fuelling the productivity of non-diazotrophs through remineralization of the added fixed N. The inclusion of atmospheric deposition (RA) stimulates productivity by about 60% with respect to the R simulation, but the stimulation (i.e. the difference between RDA and RD simulations) is weak when diazotrophs are present. N_2 fixation rates are relatively low for the D configuration (16 ± 14 μmol N m^{-2} d^{-1}) but increase by more than 300% due to the effect of enhanced phosphorus availability caused by preferential phosphorus remineralization (RD). Atmospheric deposition with high N:P ratios causes a dramatic reduction of N_2 fixation rates (RDA),

Downloaded from http://plankt.oxfordjournals.org/ by guest on July 12, 2016

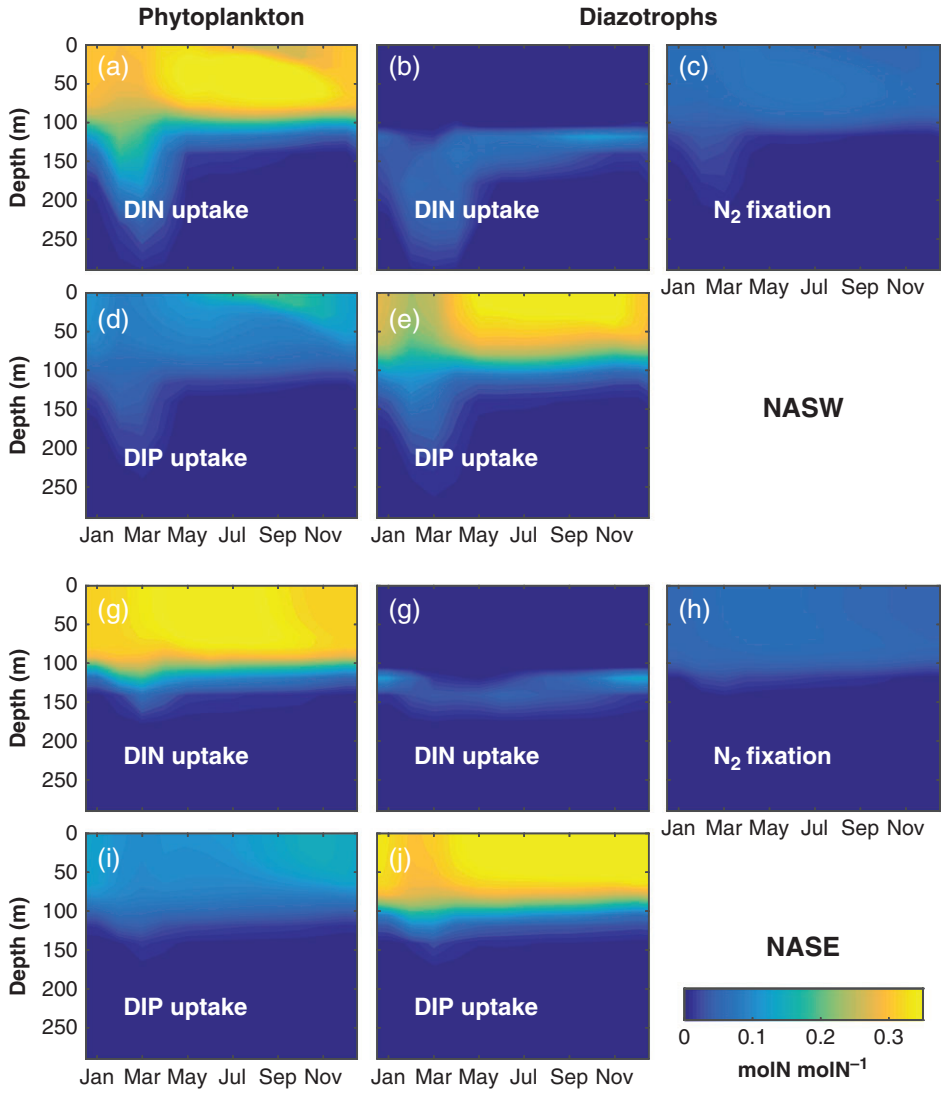

Fig. 6. Simulated relative allocation of cellular N to DIN and DIP uptake and N_2 fixation in non-diazotrophs (left) and diazotrophs (middle and right) for NASW (top) and NASE (bottom). The remaining cellular N is allocated to structural protein and enzymes for light harvesting and CO_2 fixation.

by about 42 μmol N m^{-2} d^{-1}, very similar to the amount of deposited N.

Similar to the patterns described for the NASW simulations, NPP rises by ≈71% at NASE due to the inclusion of diazotrophs (D) compared to the control (0) configuration (Fig. 7), by 136% when preferential phosphorus remineralization is also considered (RD), and it is very similar in the R and 0 configurations. The effect of the atmospheric deposition on NPP is weak in any case due to the weaker flux used for this site. The enhancement of N_2 fixation by preferential phosphorus remineralization is also significant for NASE (156%) but weaker compared to NASW. Inclusion of atmospheric deposition reduces N_2 fixation by 6.4 μmol N m^{-2} d^{-1}, which is about half of the N deposition flux. Reproduction of the observations of both NPP and N_2 fixation rates is best with the RDA simulations.

DISCUSSION

The role of oligotrophy and N:P supply ratios in controlling diazotrophy

The subtropical North Atlantic has been reported to be an area of moderate N_2 fixation activity (Luo *et al.*, 2012) with a consistent maximum of nitrate (NO_3^-) excess over the Redfield equivalent of phosphate (PO_4^{3+})

Downloaded from http://plankt.oxfordjournals.org/ by guest on July 12, 2016

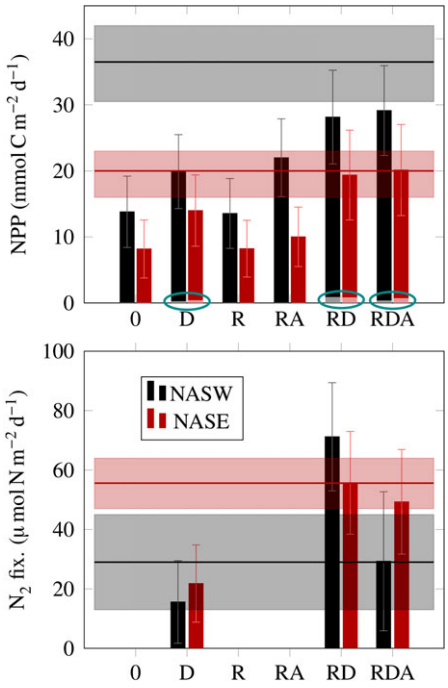

Fig. 7. Annual averages of net primary production (NPP, top) by diazotrophs (circled light coloured bars at the bottom ends of the bars for the D, RD, and RDA configurations in the upper panel) and ordinary phytoplankton (dark coloured bars), and N_2 fixation rates (bottom) simulated for the western (NASW, blacksolid bars) and eastern (NASE, redstripped bars) subtropical North Atlantic sites. Horizontal lines indicate averaged values for both stations computed from observations, and the shadowed areas and error bars represent standard deviations (see Table I for details). Model configurations include: diazotrophy (D), preferential remineralisation of phosphorus (R), and atmospheric deposition of N and P from present-day estimates (A). For the control (0) configuration none of D, R, or A are included.

in the main thermocline (150–900 m). This feature has been attributed to the remineralization of N-rich organic matter, partly resulting from diazotrophic activity. Hence, the tracer $N^* = NO_3^- - 16PO_4^{3+}$ has been used to estimate N_2 fixation rates in this region (Gruber and Sarmiento, 1997; Hansell *et al.*, 2004, 2007). This feature can be expected to exert control on diazotrophy by enhancing the N:P supply ratio into the photic layer. In fact, according to the notion that diazotrophy is ultimately coupled to N loss processes (Deutsch *et al.*, 2007), if excess P is an essential requirement for diazotrophy, the occurrence of N_2 fixation in this area cannot be explained without the existence of an external input of excess P (i.e. lateral transport in the Gulf Stream, see Palter *et al.*, 2011).

Models based on optimal phytoplankton growth have successfully reproduced phytoplankton growth in laboratory cultures (Pahlow and Oschlies, 2013) and in the open ocean (Mouriño-Carballido *et al.*, 2012; Arteaga *et al.*, 2014). These models provide a mechanistic description of phytoplankton elemental stoichiometry and physiology controlling nutrient uptake and growth, by allocating nutrients and energy such that the growth of the organism is maximized. These models represent an improvement over more traditional models with constant stoichiometry, where nutrient uptake is generally represented by Michaelis–Menten kinetics (Smith *et al.*, 2011). The recently proposed optimality-based model of phytoplankton growth and diazotrophy (Pahlow *et al.*, 2013), used in this study, offers a new interpretation of the controls of diazotrophy in plankton communities. This model appears consistent with the occurrence of diazotrophy in environments where the N:P supply ratio is higher than the Redfield ratio, and also with the finding that N_2 fixation is favoured by P limitation in terrestrial ecosystems (Houlton *et al.*, 2008). The existence of diazotrophy in high N:P supply environments is possible in the optimality-based approach under oligotrophic conditions. This is because, under nutrient starvation, diazotrophs can allocate more of their fixed N to the phosphorus acquisition machinery and successfully compete for this element (Fig. 6d,e,i and j). Thus, a major competitive advantage of the diazotrophs derives from their enhanced ability to invest in DIP uptake. As a consequence, diazotrophy is favoured both by oligotrophy, also with respect to P, and by low N:P supply ratios (see Fig. 7 in Pahlow *et al.*, 2013).

By using the optimality-based diazotrophy model described by Pahlow *et al.* (2013) we successfully reproduced seasonal patterns of diazotrophy biomass and N_2 fixation rates observed at the two sites located in the eastern (NASE) and western (NASW) subtropical North Atlantic. For that, we need to include in the simulations, at both stations, current estimates of N and P atmospheric deposition and preferential P remineralization. Although nutrients are supplied with an N:P ratio significantly higher than the Redfield ratio at both stations, especially when atmospheric deposition is considered, the oligotrophic conditions allow the occurrence of diazotrophy. Moreover, also in good agreement with the observations, our model predicts higher N_2 fixation rates at NASE. This site is characterized by a stronger degree of oligotrophy and weaker atmospheric N deposition rates (see Table I), allowing for a larger niche for diazotrophs. As a consequence, N_2 fixation rates are almost 2-fold higher at this location, compared to NASW, for the reference model run including preferential remineralization and atmospheric deposition (RDA), despite 1.5 times higher NPP rates in the west. The proportion of diazotrophs relative to ordinary phytoplankton at NASE is also higher for the reference RDA simulation (Table I, Fig. 8). This is the result of lower N:P ratios of

Downloaded from http://plankt.oxfordjournals.org/ by guest on July 12, 2016

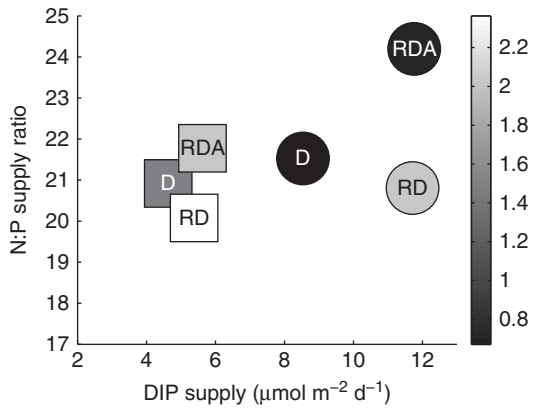

Fig. 8. Relationship between the ratio of diazotrophic phytoplankton biomass (POCD) to ordinary phytoplankton biomass (POCP), averaged DIP supply into the photic layer and N:P ratios of the nutrient supply (including vertical mixing and atmospheric deposition) for the different model configurations at NASW (circles) and NASE (squares): diazotrophy (D), preferential remineralisation of phosphorus (R), and atmospheric deposition of N and P from present-day estimates (A).

the physical supply (due to weaker atmospheric deposition), and the lower nutrient supply into the photic layer at the NASE site (Fig. 8). Furthermore, due to the weaker physical supply of new N, both through transport across the thermocline and atmospheric deposition, diazotrophy plays a more important role at NASE, supplying 29% of the newly available N, whereas it contributes only 10% at NASW. This fact highlights the more important role of diazotrophy for new production in the eastern station. These results agree with the findings of Luo *et al.* (2012) and Fernández *et al.* (2012), who found a west to east increase in diazotrophy in the subtropical North Atlantic.

Interaction between diazotrophy, preferential P remineralization and atmospheric deposition

Recently, based on the compilation of global measurements of DOM concentration, Letscher and Moore (2015) demonstrated that phosphorus is remineralized 1.5–3 times faster than N in the upper ocean, and that this trend is more pronounced in the North Atlantic basin, where N_2 fixation is also important (Luo *et al.*, 2012). Previous studies already demonstrated the importance of faster P cycling in this region (Wu *et al.*, 2000), and also pointed at this mechanism as a possible contributor, together with N_2 fixation, to the development of the nitrate excess in the thermocline (Monteiro and Follows, 2012). Letscher and Moore (2015) also suggested a close interaction between diazotrophy and preferential remineralization of phosphorus, as this mechanism could stimulate diazotrophy and primary production. Sensitivity simulations carried out with our different model configurations indicate that faster P recycling can significantly increase N_2 fixation and improve the reproduction of its seasonality.

Rapid recycling of P increases its availability during the late summer months, making it available for diazotrophs and increasing the rate of N_2 fixation during this period (RD and RDA simulations). In the D simulation (without preferential P remineralization), P availability is too low during late summer and autumn, and maximum fixation occurs in winter and spring, when P availability is enhanced by deep mixing. This seasonal pattern is opposite to the observed pattern at BATS (Fig. 5a). Including this process is also essential to achieve a good reproduction of the observed NPP and N_2 fixation rates at both sides of the subtropical North Atlantic (Fig. 7). Preferential remineralization increases phosphorus supply to the photic layer, resulting in a lower N:P ratio of the supply (Fig. 8). As oligotrophy is relieved in this case, and the N:P supply ratios across the thermocline are only slightly reduced, preferential P remineralization also reduces the N:P of the nutrient supply resulting from remineralization processes within the photic zone, enhancing the competitive advantage of diazotrophs. Thus, this process is relatively most effective during stratified conditions in summer and causes a peak in integrated N_2 fixation towards late summer/early autumn (Fig. 5e and f). Lowering the N:P supply below Redfield proportions via preferential P remineralization has been the mechanism creating the niche for diazotrophs in previous modelling studies (Zamora *et al.*, 2010; Letscher and Moore, 2015). By contrast, diazotrophy is favoured also by oligotrophy with respect to P, owing to the high competitive ability for P of the diazotrophs (Fig. 6e and j), so that diazotrophy is compatible with much higher N:P supply ratios in our approach.

In our simulations atmospheric deposition results in an increase in the N:P ratio of the physical nutrient supply (Fig. 8), and, as a consequence, causes a decrease of N_2 fixation rates (Figs. 5 and 7). Again, NASW is more sensitive to this flux both because it departs from an already reduced diazotrophy niche in comparison to NASE and also because atmospheric N deposition estimates are higher for this location. Atmospheric deposition (whether constant or temporally variable) shifts N_2 fixation even further towards the late summer/early autumn peak compared to the RD simulation, which agrees better with the observations (Fig. 5). Owing to the high N:P ratio of the atmospheric deposition, the N:P supply ratio is raised most strongly at the surface and hence not only reduces overall N_2 fixation but also pushes the peak down below the bottom of the mixed layer. A subsurface niche for diazotrophs may, at first

Downloaded from http://plankt.oxfordjournals.org/ by guest on July 12, 2016

sight, look counter-intuitive. However, comparison with Fig. 3 reveals that this N_2 fixation occurs well above the nitracline at both sites, where primary production is still strongly limited by N supply. The N from atmospheric deposition is utilized within the mixed layer, and N from below the nitracline cannot move upwards due to a lack of mixing. Thus, the diazotroph niche comes to exist between the bottom of the mixed layer and the top of the nitracline. This does not happen during the winter-mixing period at BATS, because at that time N supply from below prevents the generation of a subsurface niche for diazotrophs.

The interaction between N_2 fixation and atmospheric deposition of high N:P matter is particularly critical as significant increases of atmospheric N deposition are predicted for the coming decades (Duce *et al.*, 2008). We further investigate this interaction at both sites by simulating scenarios of progressively enhanced N input from the atmosphere, ranging from 0 to 4 (NASW) and from 0 to 6 (NASE) times the respective present-day estimates of atmospheric deposition (Fig. 9). The upper limit might not be realistic in the near future, but human activity might lead to increments by a factor of about 1.5 for large areas of the North Atlantic within the next 20 years (Duce *et al.*, 2008). In the absence of preferential P remineralization, the estimated present-day deposition of N can already destroy the niche for diazotrophs at NASW (not shown). All simulations in Fig. 9 include preferential remineralization of phosphorus, and even in this case, a deposition of about 80 μmol N m^{-2} d^{-1}, less than twice the present-day estimate, completely suppresses N_2 fixation at NASW. However, for the NASE site, where the present estimate of atmospheric N deposition is lower, a 6-fold increase in atmospheric deposition (ca. 70 μmol N m^{-2} d^{-1}) will be needed to suppress N_2 fixation. At both sites, the effect of increasing atmospheric deposition on N_2 fixation could be either stronger or weaker compared to Fig. 9, depending on the seasonal distribution of the additional atmospheric deposition.

Pahlow *et al.* (2013) describe an emerging feature resulting from a community of competing diazotrophic and non-diazotrophs, controlling ambient DIN:DIP ratios and decoupling them from the supply ratio. The optimal ratio of DIN and DIP uptake in the chain model depends on ambient DIN and DIP concentrations and is much higher than the Redfield ratio for non-diazotrophs in the present model simulations (about 27, Table I). Owing to the fact that diazotrophs do not require fixed N for growth, the fixed N is eventually, i.e. after being recycled through grazing and remineralization, utilized by non-diazotrophs. Due to the high cost of N_2 fixation, the competition between diazotrophs and non-diazotrophs thus leads to a strong dominance of the non-diazotrophs. Still, the diazotroph's niche appears stable, as it persists throughout our simulations unless atmospheric N deposition is too high.

Since the main effect of the N_2 fixation is an amplification of primary production by the non-diazotrophs,

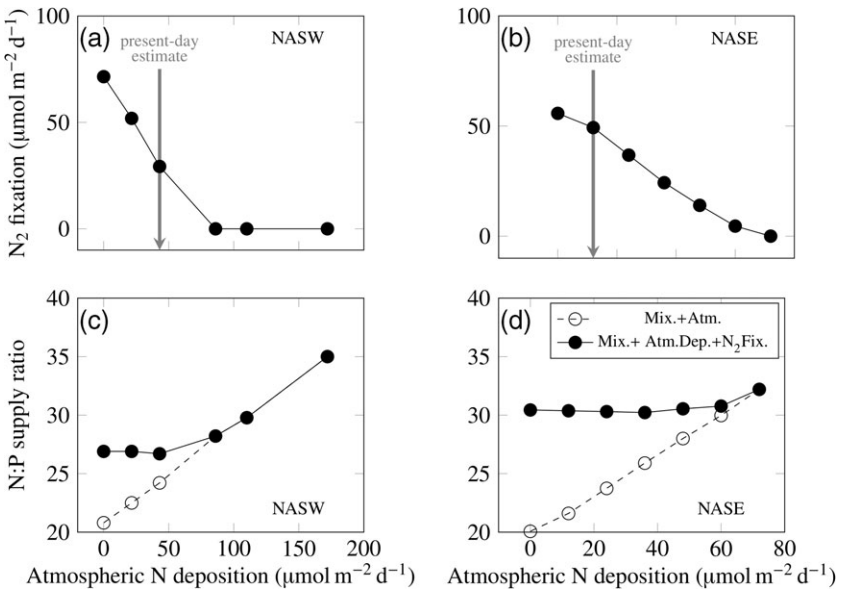

Fig. 9. Relationship between atmospheric N deposition and (a,b) simulated N_2 fixation rates and (c,d) the N:P supply ratio for the reference RDA configuration (including diazotrophy, preferential remineralisation of phosphorus and atmospheric N deposition) at the NASW and NASE sites. Two different N:P supply ratios are considered, one including only vertical mixing and atmospheric deposition (o) and another one also including biological N2 fixation (●).

Downloaded from http://plankt.oxfordjournals.org/ by guest on July 12, 2016

the very weak effect of the diazotrophs on DIN:DIP is overridden by the much stronger effect of the high DIN:DIP uptake ratio of the non-diazotrophs, which drives ambient DIN:DIP ratios towards values lower than Redfield. Thus, despite the high total N:P supply ratios (26.8 and 33.2 for NASW and NASE, respectively), the DIN:DIP ratios in the euphotic zone for our reference simulation, are 12 and 14 for NASW and NASE, respectively, in close agreement with the observations. This would not be possible if DIN and DIP were utilized in Redfield proportions, which would necessarily raise ambient DIN:DIP ratios above the supply ratio. Due to low nutrient concentrations in the subtropical surface oceans, the DIN:DIP ratios are difficult to determine accurately enough to confidently validate the model. The averaged ratio of nitrate ($NO_3 + NO_2$) to phosphate (PO_4) calculated with data from the BATS site is 24, very similar to the supply ratio. However, when low-level (nano-molar) P determinations (reported as soluble reactive phosphorus) are considered, this ratio drops to 13, in close agreement with the model.

Our simulations with increasing N deposition, which result in progressively enhanced N:P ratios of the physical (mixing + deposition) nutrient supply, indicate that diazotrophy also controls the N:P ratio of the total supply, including physical processes and N_2 fixation (Fig. 9). At NASW, the total N:P supply ratio is about 27, well above Redfield, except at high N atmospheric deposition when the N:P ratio is higher than this value and diazotrophy is suppressed. At NASE, the total N:P supply ratio is 30 in all simulations including diazotrophy, sensibly higher compared to NASW. This is likely the result of the most favourable niche for diazotrophs provided by the more oligotrophic conditions at NASE, as indicated by the much lower DIN and DIP fluxes (Table I). Despite these more favourable conditions for diazotrophy at NASE, an atmospheric deposition flux of about 70 μmol N m^{-2} d^{-1} would be enough to cause $(N:P)_{supply}$ »30 and suppress N_2 fixation. The atmospheric flux needed to suppress nitrogen fixation is slightly lower compared to NASW due to the weaker phosphorus input. These results suggest that the increase in atmospheric deposition of N predicted for the next century (Duce *et al.*, 2008) could potentially have a strong negative effect on marine diazotrophy, possibly counteracting the favourable conditions generated by the expansion of warm and well-stratified areas of the ocean (Polovina *et al.*, 2008).

OUTLOOK

Atmospheric N_2 fixation by marine diazotrophs contributes to the productivity of nutrient-poor subtropical gyres and their capacity for carbon export (Beckmann and Hense, 2009). Due to the predicted expansion of oligotrophic ocean areas as a consequence of global warming (Polovina *et al.*, 2008), this process is likely to play an important role in the evolution of the marine biological carbon pump in the near future. Despite its importance, the large-scale controls on the distribution of diazotrophy are still uncertain (Luo *et al.*, 2014). The development of an optimality-based approach to model diazotrophy in oceanic phytoplankton (Pahlow *et al.*, 2013) has challenged the simplistic notion that N_2 fixation is favoured by an excess of P in the surface ocean (Deutsch *et al.*, 2007). This view has also been difficult to reconcile with observations of significant diazotrophic activity in the P-depleted tropical and subtropical North Atlantic Ocean (Palter *et al.*, 2011). Our optimality-based model predicts that diazotrophy is associated with oligotrophy, also with respect to P, as diazotrophic phytoplankton can allocate more N into the P-acquisition machinery (Houlton *et al.*, 2008). Diazotrophs have been suggested to benefit from the ability to utilize DOP (Dyhrman *et al.*, 2006), which is not explicitly accounted for in our model. The ability to use DOP is likely linked to the high N availability in diazotrophs (Houlton *et al.*, 2008), and could thus be viewed as an amplification of the competitive ability for P relative to non-diazotrophs (Landolfi *et al.*, 2015; Somes and Oschlies, 2015). Our optimality-based model is able to reproduce the observed levels of N_2 fixation in the western (NASW) and eastern (NASE) North Atlantic subtropical gyre, characterized by higher than Redfield N:P ratios of new nutrient supply. These results demonstrate the advantage of the physiologically meaningful optimal growth approach, over more traditional mechanistic models (Bissett *et al.*, 1999; Hood *et al.*, 2001; Agawin *et al.*, 2007), to predict the importance of diazotrophy in oligotrophic oceans. It is important to note that our model was calibrated to reproduce the observed behaviour of the non-heterocystous colony-forming diazotrophic cyanobacterium *Trichodesmium* sp., traditionally considered a major contributor to N_2 fixation in the subtropical North Atlantic. However, more recently the wide distribution of unicellular free living and symbiont N_2 fixers has been reported (Zehr, 2011), broadening the ecological niche of diazotrophy and expanding its geographical domain (Sohm *et al.*, 2011). In addition, neglecting iron in our model restricts its application to regions with high iron supply, such as the North Atlantic (Jickells *et al.*, 2005). More studies about the physiological characteristics of these organisms and the main factors controlling their distribution are needed in order to include them in ecological models and improve our understanding of the role of diazotrophy in the marine and global N cycle.

Downloaded from http://plankt.oxfordjournals.org/ by guest on July 12, 2016

SUPPLEMENTARY DATA

Supplementary data can be found online at http://plankt.oxfordjournals.org

ACKNOWLEDGEMENTS

The authors gratefully acknowledge valuable and helpful comments from R. Letelier and two anonymous reviewers, which have greatly improved the manuscript. This work is a contribution of the Sonderforschungsbereich 754 "Climate-Biogeochemistry Interactions in the Tropical Ocean" (http://www.sfb754.de), which is funded by the German Science Foundation (DFG).

FUNDING

Funding for this study was also provided by the Xunta de Galicia under the research projects VARITROP (09MDS001312PR) and NICANOR (EM2013/021) to B. M.-C. B. F.-C. thanks to the Spanish government for a FPU grant (AP2010-5594) and a travel grant (Est13/01044). M. P. acknowledges support by the CREST project (PI: S. L. Smith) funded by the Japan Science Foundation.

REFERENCES

Agawin, N. S. R., Rabouille, S., Veldhuis, M. J. W., Servatius, L., Hol, S., Overzee, M. J. V. and Huisman, J. (2007) Competition and facilitation between unicellular nitrogen–fixing cyanobacteria and non–nitrogen-fixing phytoplankton species. *Limnol. Oceanogr.*, **52**, 2233–2248.

Arteaga, L., Pahlow, M. and Oschlies, A. (2014) Global patterns of phytoplankton nutrient and light colimitation inferred from an optimality-based model. *Global. Biogeochem. Cycles*, **28**, 648–661.

Arteaga, L., Pahlow, M. and Oschlies, A. (2015) Global monthly sea surface nitrate fields estimated from remotely sensed sea surface temperature, chlorophyll, and modeled mixed layer depth. *Geophys. Res. Lett.* **42**, 1130–1138.

Beckmann, A. and Hense, I. (2009) A fresh look at the nutrient cycling in the oligotrophic ocean. *Biogeochemistry*, **96**, 1–11.

Bibby, T. S. and Moore, C. M. (2011) Silicate:nitrate ratios of upwelled waters control the phytoplankton community sustained by mesoscale eddies in sub-tropical North Atlantic and Pacific. *Biogeosciences*, **8**, 657–666.

Bissett, W. P., Carder, K. L., Walsh, J. J. and Dieterle, D. A. (1999) Carbon cycling in the upper waters of the Sargasso Sea: II. Numerical simulation of apparent and inherent optical properties. *Deep-Sea Res. I*, **46**, 271–317.

Brix, H., Gruber, N., Karl, D. M. and Bates, N. R. (2006) On the relationships between primary, net community, and export production in subtropical gyres, *Deep Sea. Res. II*, **53**, 698–717.

Capone, D. G., Burns, J. A., Montoya, J. P., Subramaniam, A., Mahaffey, C., Gunderson, T., Michaels, A. F., and Carpenter, E. J. (2005) Nitrogen fixation by *Trichodesmium* spp.: an important source of new nitrogen to the tropical and subtropical north atlantic ocean. *Global. Biogeochem. Cycles*, **19**, GB2024.

Carpenter, E. J. (1983) Physiology and ecology of marine planktonic Oscillatoria (Trichodesmium*). Mar. Biol. Lett.*, **4**, 69–85.

Carpenter, E. J. and Capone, D. G. (2008) Nitrogen fixation in the marine environment. In *Nitrogen in the Marine Environment.* Elsevier Inc., Burlington, Mass. pp. 141–198.

Cianca, A., Santana, R., Hartman, S., Martín-González, J., González-Dávila, M., Rueda, M., Llinás, O. and Neuer, S. (2013) Oxygen dynamics in the North Atlantic subtropical gyre. *Deep Sea Res. II*, **93**, 135–147.

Deutsch, C., Sarmiento, J. L., Sigman, D. M., Gruber, N. and Dunne, J. P. (2007) Spatial coupling of nitrogen inputs and losses in the ocean. *Nature*, **445**, 163–7.

Duce, R. A., LaRoche, J., Altieri, K., Arrigo, K. R., Baker, A. R., Capone, D. G., Cornell, S., Dentener, F., *et al.* (2008) Impacts of atmospheric anthropogenic nitrogen on the open ocean. *Science*, **320**, 893–897.

Dyhrman, S. T., Chappell, P. D., Haley, S. T., Moffett, J. W., Orchard, E. D., Waterbury, J. B. and Webb, E. A. (2006) Phosphonate utilization by the globally important marine diazotroph *Trichodesmium*. *Nature*, **439**, 68–71.

Emerson, S., Quay, P., Karl, D., Winn, C., Tupas, L. and Landry, M. (1997) Experimental determination of the organic carbon flux from open-ocean surface waters. *Nature*, **389**, 951–954.

Fernández, A., Graña, R., Mouriño-Carballido, B., Bode, A., Varela, M., Dominguez-Yanes, J. F., Escánez, J., de Armas, D., *et al.* (2012) Community N_2 fixation and *Trichodesmium* spp. abundance along longitudinal gradients in the eastern subtropical North Atlantic. *ICES J. Mar. Sci.*, **70**, 223–231.

Fernández, A., Mouriño-Carballido, B., Bode, A., Varela, M. and Marañón, E. (2010) Latitudinal distribution of *Trichodesmium* spp. and N_2 fixation in the Atlantic Ocean. *Biogeosciences*, **7**, 3167–3176.

Fernández-Castro, B., Anderson, L., Marañón, E., Neuer, S., Ausín, B., Gonzáez-Dávila, M., Santana-Casiano, J. M., Cianca, A., *et al.* (2012) Regional differences in modelled net production and shallow remineralization in the North Atlantic subtropical gyre. *Biogeosciences*, **9**, 2831–2846.

Fernández-Castro, B., Mouriño-Carballido, B., Marañón, E., Chouciño, P., Gago, J., Ramírez, T., Vidal, M., Bode, A., *et al.* (2015) Importance of salt fingering for new nitrogen supply in the oligotrophic ocean. *Nat. Commun.*, **6**, 8002.

Field, C. B., Behrenfeld, M. J., Randerson, J. T. and Falkowski, P. (1998) Primary production of the biosphere: Integrating terrestrial and oceanic components. *Science*, **281**, 237–240.

Garcia, H. E., Locarnini, R. A., Boyer, T., Antonov, J. I., Zweng, M. and Johnson, D. R. (2010) *World Ocean Atlas 2009, Volume 4: Nutrients (phosphate, nitrate, silicate).* NOAA Atlas NESDIS 71, U.S. Government Printing Office, Washington, D.C.

González-Dávila, M., Santana-Casiano, J. M. and González-Dávila, E. F. (2007) Interannual variability of the upper ocean carbon cycle in the northeast Atlantic Ocean, *Geophys. Res. Lett.*, **34**, L07608.

Gruber, N., Keeling, C. D. and Stocker, T. F. (1998) Carbon-13 constraints on the seasonal inorganic carbon budget at the BATS site in the northwestern Sargasso Sea. *Deep-Sea Res. I*, **45**, 673–717.

Downloaded from http://plankt.oxfordjournals.org/ by guest on July 12, 2016

Gruber, N. and Sarmiento, J. L. (1997) Global patterns of marine nitrogen fixation and denitrification. *Global. Biogeochem. Cycles*, **11**, 235–266.

Guieu, C., Aumont, O., Paytan, A., Bopp, L., Law, C. S., Mahowald, N., Achterberg, E. P., Marañón, E., *et al.* (2014) The significance of the episodic nature of atmospheric deposition to Low Nutrient Low Chlorophyll regions. *Global. Biogeochem. Cycles*, **28**, 1179–1198.

Hansell, D. A., Bates, N. R. and Olson, D. B. (2004) Excess nitrate and nitrogen fixation in the North Atlantic Ocean. *Mar.Chem.*, **84**, 243–265.

Hansell, D. A., Olson, D. B., Dentener, F. and Zamora, L. M. (2007) Assessment of excess nitrate development in the subtropical North Atlantic. *Mar. Chem.*, **106**, 562–579.

Helmke, P., Neuer, S., Lomas, M. W., Conte, M. and Freudenthal, T. (2010) Cross-basin differences in particulate organic carbon export and flux attenuation in the subtropical North Atlantic gyre. *Deep-Sea Res. I*, **57**, 213–227.

Hood, R. R., Bates, N. R., Capone, D. G. and Olson, D. B. (2001) Modeling the effect of nitrogen fixation on carbon and nitrogen fluxes at BATS. *Deep-Sea Res. II*, **48**, 1609–1648.

Houlton, B. Z., Wang, Y.-P., Vitousek, P. M. and Field, C. B. (2008) A unifying framework for dinitrogen fixation in the terrestrial biosphere. *Nature*, **454**, 327–30.

Jickells, T. D., An, Z. S., Andersen, K. K., Baker, A. R., Bergametti, G., Brooks, N., Cao, J. J., Boyd, P. W., *et al.* (2005) Global iron connections between desert dust, ocean biogeochemistry, and climate. *Science*, **308**, 67–71.

Krauk, J. M., Villareal, T. A., Sohm, J. A., Montoya, J. P. and Capone, D. G. (2006) Plasticity of N:P ratios in laboratory and field populations of. *Limnol. Oceanogr.*, **42**, 243–253.

Krishnamurthy, A., Moore, J. K., Zender, C. S. and Luo, C. (2007) Effects of atmospheric inorganic nitrogen deposition on ocean biogeochemistry. *J. Geophys. Res.*, **112**, 1–10.

Landolfi, A., Dietze, H., Koeve, W. and Oschlies, A. (2013) Overlooked runaway feedback in the marine nitrogen cycle: the vicious cycle. *Biogeosciences*, **10**, 1351–1363.

Landolfi, A., Koeve, W., Dietze, H., Kaehler, P. and Oschlies, A. (2015) A new perspective on environmental controls of marine nitrogen fixation. *Geophys. Res. Lett.*, **42**, 4482–4489.

Letelier, R. and Karl, D. (1998) *Trichodesmium* spp. physiology and nutrient fluxes in the North Pacific subtropical gyre. *Aquat. Microb. Ecol.*, **15**, 265–276.

Letscher, R. and Moore, J. (2015) Preferential remineralization of dissolved organic phosphorus and non-Redfield DOM dynamics in the global ocean. *Glob. Biogeochem. Cycles*, **29**, 325–340.

Luo, Y.-W., Doney, S. C., Anderson, L. A., Benavides, M., Bode, A., Bonnet, S., Boström, K. H., Böttjer, D., *et al.* (2012) Database of diazotrophs in global ocean: abundance, biomass and nitrogen fixation rates. *Earth Syst. Sci. Data*, **4**, 47–73.

Luo, Y. W., Lima, I. D., Karl, D. M., Deutsch, C. A. and Doney, S. C. (2014) Data-based assessment of environmental controls on global marine nitrogen fixation. *Biogeosciences*, **11**, 691–708.

Mahowald, N., Jickells, T. D., Baker, A. R., Artaxo, P., Benitez-Nelson, C. R., Bergametti, G., Bond, T. C., Chen, Y., *et al.* (2008) Global distribution of atmospheric phosphorus sources, concentrations and deposition rates, and anthropogenic impacts. *Global. Biogeochem. Cycles*, **22**, GB4026.

Marañón, E., Pérez, V., Fernández, E., Anadón, R., Bode, A., González, N., Huskin, I. n., Isla, A., *et al.* (2007) Planktonic carbon budget in the eastern subtropical North Atlantic. *Aquat. Microb. Ecol.*, **48**, 261–275.

Marchal, O., Monfray, P. and Bates, N. R. (1996) Spring summer imbalance of dissolved inorganic carbon in the mixed layer of the northwestern Sargasso Sea, *Tellus B-Chem. Phys. Meteorol.*, **48**, 115–134.

Mills, M., Ridame, C., Davey, M., Roche, J. L. and Geider, R. (2004) Iron and phosphorus co-limit nitrogen fixation in the eastern tropical North Atlantic. *Nature*, **429**, 292–294.

Monteiro, F. M. and Follows, M. J. (2012) On nitrogen fixation and preferential remineralization of phosphorus. *Geophys. Res. Lett.*, **39**, L06607.

Moore, C. M., Mills, M. M., Achterberg, E. P., Geider, R. J., LaRoche, J., Lucas, M. I., McDonagh, E. L., Pan, X., *et al.* (2009) Large-scale distribution of Atlantic nitrogen fixation controlled by iron availability. *Nat. Geosci.*, **2**, 867–871.

Moore, C. M., Mills, M. M., Arrigo, K. R., Berman-Frank, I., Bopp, L., Boyd, P. W., Galbraith, E. D., Geider, R. J., *et al.* (2013) Processes and patterns of oceanic nutrient limitation. *Nat. Geosci.*, **6**, 701–710.

Mouriño-Carballido B. (2009) Eddy-driven pulses of respiration in the Sargasso Sea. *Deep Sea Res. I*, **56**, 1242–1250.

Mouriño-Carballido, B., Graña, R., Fernández, A., Bode, A., Varela, M., Domínguez, J. F., Escánez, J., de Armas, D., *et al.* (2011) Importance of N_2 fixation vs. nitrate eddy diffusion along a latitudinal transect in the Atlantic Ocean. *Limnol. Oceanogr.*, **56**, 999–1007.

Mouriño-Carballido, B., Pahlow, M. and Oschlies, A. (2012) High sensitivity of ultra-oligotrophic marine ecosystems to atmospheric nitrogen deposition. *Geophys. Res. Lett.*, **39**, L05601.

Musgrave, D. L., Chou, J. and Jenkins, W. J. (1988) Application of a model of upper-ocean physics for studying seasonal cycles of oxygen, *J. Geophys. Res.*, **93**, 15679–15700.

Neuer, S., Cianca, A., Helmke, P., Freudenthal, T., Davenport, R., Meggers, H., Knoll, M., Santana-Casiano, J. M., *et al.* (2007) Biogeochemistry and hydrography in the eastern subtropical North Atlantic gyre. Results from the European time-series station ESTOC. *Prog. Oceanogr.*, **72**, 1–29.

Orcutt, K. M., Lipschultz, F., Gundersen, K., Arimoto, R., Michaels, A. F., Knap, A. H., and Gallon, J. R. (2001) A seasonal study of the significance of N2 fixation by Trichodesmium spp. at the Bermuda Atlantic Time-series Study (BATS) site. *Deep Sea Res. II*, **48**, 1583–1608.

Oschlies, A. and Garçon, V. (1999) An eddy-permitting coupled physical-biological model of the North Atlantic. 1. Sensitivity to advection numerics and mixed layer physics. *Global. Biogeochem. Cycles*, **13**, 135–160.

Pahlow, M., Dietze, H., and Oschlies, A. (2013) Optimality-based model of phytoplankton growth and diazotrophy. *Mar. Ecol. Prog. Ser.*, **489**, 1–16.

Pahlow, M. and Oschlies, A. (2013) Optimal allocation backs Droop's cell-quota model. *Mar. Ecol. Prog. Ser.*, **473**, 1–5.

Pahlow, M. and Prowe, A. (2010) Model of optimal current feeding in zooplankton. *Mar. Ecol. Prog. Ser.*, **403**, 129–144.

Pahlow, M., Vézina, A. F., Casault, B., Maass, H., Malloch, L., Wright, D. G. and Lu, Y. (2008) Adaptive model of plankton dynamics for the North Atlantic. *Prog. Oceanogr.*, **76**, 151–191.

Painter, S. C., Patey, M. D., Forryan, A. and Torres-Valdes, S. (2013) Evaluating the balance between vertical diffusive nitrate

Downloaded from http://plankt.oxfordjournals.org/ by guest on July 12, 2016

supply and nitrogen fixation with reference to nitrate uptake in the eastern subtropical North Atlantic Ocean. *J. Geophys. Res.*, **118**, 5732–5749.

Palter, J. B., Lozier, M. S., Sarmiento, J. L. and Williams, R. G. (2011) The supply of excess phosphate across the Gulf Stream and the maintenance of subtropical nitrogen fixation. *Global. Biogeochem. Cycles*, **25**, GB4007.

Polovina, J. J., Howell, E. A., and Abecassis, M. (2008) Ocean's least productive waters are expanding. *Geophys. Res. Lett.*, **35**, L03618.

Saba, V. S., Friedrichs, M. A. M., Carr, M.-E., Antoine, D., Armstrong, R. A., Asanuma, I., Aumont, O., Bates, N. R., *et al.* (2010) Challenges of modeling depth-integrated marine primary productivity over multiple decades: a case study at bats and hot. *Global. Biogeochem. Cycles*, **24**, GB3020.

Salihoglu, B., Garçon, V., Oschlies, A. and Lomas, M. W. (2008) Influence of nutrient utilization and remineralization stoichiometry on phytoplankton species and carbon export: a modeling study at BATS. *Deep-Sea Res. I*, **55**, 73–107.

Sañudo-Wilhelmy, S. and Kustka, A. (2001) Phosphorus limitation of nitrogen fixation by *Trichodesmium* in the central Atlantic Ocean. *Nature*, **411**, 66–69.

Siegel, D. A., McGillicuddy, D. J. Jr. and Fields, E. A. (1999) Mesoscale eddies, satellite altimetry, and new production in the Sargasso Sea. *J. Geophys. Res.*, **104**(C6), 13359–13379.

Smith, S. L., Pahlow, M., Merico, A. and Wirtz, K. W. (2011) Optimality-based modeling of planktonic organisms. *Limnol. Oceanogr.*, **56**, 2080–2094.

Sohm, J. A., Webb, E. A. and Capone, D. G. (2011) Emerging patterns of marine nitrogen fixation. *Nat. Rev. Microbiol.*, **9**, 499–508.

Somes, C. J. and Oschlies, A. (2015) On the influence of "non-Redfield" dissolved organic nutrient dynamics on the spatial distribution of N_2 fixation and the size of the marine fixed nitrogen inventory. *Global. Biogeochem. Cycles*, **29**, 973–993.

Steinberg, D. K., Carlson, C. A., Bates, N. R., Johnson, R. J., Michaels, A. F. and Knap, A. H. (2001) Overview of the US JGOFS Bermuda Atlantic Time-series Study (BATS): a decade-scale look at ocean biology and biogeochemistry. *Deep Sea Res. II*, **48**, 1405–1447.

Sterner, R. W. and Elser, J. J. (2002) *Ecological stoichiometry: the biology of elements from molecules to the biosphere.* Princeton Univ. Press, Princeton, NJ, USA.

Wu, J., Sunda, W., Boyle, E. and Karl, D. (2000) Phosphate depletion in the western North Atlantic *Ocean*. Science, **289**, 759–763.

Zamora, L., Landolfi, A., and Oschlies, A. (2010) Atmospheric deposition of nutrients and excess N formation in the North Atlantic. *Biogeosciences*, **1**, 777–793.

Zehr, J. P. (2011) Nitrogen fixation by marine cyanobacteria. *Trends. Microbiol.*, **19**, 162–73.

Downloaded from http://plankt.oxfordjournals.org/ by guest on July 12, 2016